Experimental and Numerical Investigation of Wake-Induced Transition on a Highly Loaded LP Turbine at Low Reynolds Numbers

Conference Paper · May 2000

DOI: 10.1115/2000-GT-0269

3 authors, including:

Andreas Fiala
MTU Aero Engines
18 PUBLICATIONS **222** CITATIONS

EXPERIMENTAL AND NUMERICAL INVESTIGATION OF WAKE-INDUCED TRANSITION ON A HIGHLY LOADED LP TURBINE AT LOW REYNOLDS NUMBERS

Peter Stadtmüller, Leonhard Fottner

Institut für Strahlantriebe
Universität der Bundeswehr München
D-85577 Neubiberg
Germany

Andreas Fiala

MTU Motoren- und
Turbinen-Union München GmbH
D-80995 München
Germany

ABSTRACT

Experimental and numerical results of LP turbine cascade tests performed to investigate wake interaction effects on boundary layer transition are presented. The data obtained at different inlet flow angles, turbulence levels and Mach numbers are compared and discussed with special focus on low Reynolds number conditions. For the boundary layer, calculated propagation velocities of disturbances are introduced to explain the transition process on the suction side of the blade over time.

Using a moving bar wake generator and surface-mounted hot films as well as surface pressure tappings, the effects of periodic wake passing were studied in the High-Speed Cascade Wind Tunnel on the aft-loaded LPT profile T106. Blade pitch was increased as compared with design point conditions to achieve a higher blade loading. As a result, a large separation bubble formed on the suction side of the surface and allowed unsteady boundary layer development to be studied in great detail. Starting at a characteristic Reynolds number, massive separation occurred on the suction side under steady state conditions, i.e. the boundary layer was unable to reach the back pressure at the trailing edge. By using the wake generator, it was possible to reduce this separation and thus decrease profile pressure losses by 50%.

The primary objective of the study was to provide unsteady ensemble-averaged hot film data together with information on the wake induced path, sufficient for the validation of numerical simulations. Such a simulation of the experiment was conducted using the Unsteady Boundary Layer Interaction Method, which takes into account the influence of boundary layer displacement on the velocity distribution and the time-dependent turbulence level in the outflow. The computations provide a good description of the wall shear stress in the transitional region and are in good agreement with the experimental data. By plotting propagation directions of boundary layer disturbances in space-time diagrams, it is shown that one characteristic direction is deviated around the so-called becalmed region and the temporarily separated region into the wake-induced transitional region.

NOMENCLATURE

Latin

BL	Boundary Layer
c	velocity [m/s]
c_f	skin friction coefficient = f(θ,H)
c_d	dissipation coefficient = f(θ,H)
d	diameter [m]
CTA	Constant Temperature Anemometry
E	anemometer output voltage
EIZ	Generator of unsteady inlet flow conditions
f	frequency $f = U/t_b$
h	blade height [m]
H	shape factor
H^*	kinetic energy shape factor = f(θ,H)
l	chord length [m]
LPT	Low Pressure Turbine
Ma	Mach number

p	pressure [hPa]
PLEAT	Phase Locked Ensemble Averaging Technique
Re	Reynolds number Re = c·l/ν
RMS	Root Mean Square
Sr	Strouhal number Sr = f·l/c_{ax}
T	time period between two wakes [s]
Tu	turbulence level [%]
t	time[s], pitch [m]
u	velocity component tangential to the blade surface [m/s]
U	bar velocity [m/s]
x	blade surface position [m]

For further definitions of BL quantities see Arndt (1991)

Greek

β	flow angle [°]
μ_3	skewness
ν	kinematic viscosity [m^2/s]
ω	stagnation pressure loss coefficient
θ	momentum thickness

Superscripts, Subscripts

~	ensemble-averaged
∞, e	freestream conditions, at the edge of the BL
0	at zero flow conditions
1	cascade inlet plane
2th	cascade exit plane (isentropic flow conditions)
ax	axial
b	bar
is	isentropic
k	incompressible property
o	at separation
t	total

INTRODUCTION

Recent research has indicated that the BL development on axial turbomachine blades is dominated by unsteady effects associated with blade wakes and secondary vorticies. Unpredicted low losses at typical cruise Reynolds numbers stimulated the interest in wake-induced transition and separation mechanisms on highly loaded LP turbine blades. Experimental data showed that due to the increased level of turbulence, the transition on the suction side moves upstream whenever an incoming wake is present on the surface. It was generally assumed that the increased fraction of blade surface area covered by turbulent flow results in higher profile losses, which was experimentally confirmed by Hodson (1984).

Newer investigations support the view that transitional patches in conjunction with becalmed regions and regions of temporaily separated flow lead to an overall decrease in stagnation pressure loss and to improved heat transfer coefficients. A tailored high-lift blade design accounting for rotor-stator interaction could allow for increased blade loading, resulting in a smaller number of blades per stage and thus in reduced weight and specific fuel consumption. As LPTs usually consist of several stages of considerable mass, the incentive for improving this component is large.

Many researchers studied different aspects of rotor-stator interaction, often by simulating upstream blade rows with bars (e.g. Pfeil et al., (1983), Hodson (1984), Schulte et al. (1998)). They showed that unsteady BL development has a significant impact on the profile loss distribution. However, most of these investigations did not account for turbomachinery environments, i.e. realistic Mach- and Reynolds number conditions.

The available experimental data led to a number of wake-induced transition models of which the most popular are those by Hodson (1989, 1992) and Mayle and Dullenkopf (1990). Hodson's early simple model is based on the impact of wake-induced transition on profile loss and assumes that due to the high turbulence intensity in the wake, a uniform turbulent band which propagates at the local freestream velocity develops at a certain distance from the leading edge. In the model proposed by Mayle and Dullenkopf, the wake generates turbulent spots that merge to form a turbulent strip. Contrary to Hodson's model, this strip grows along the surface *independent* of the wake at celerity rates similar to those of conventional turbulent spots. Hodson's later model extends his previous one in a way to be consistent with the turbulent spot theory. It now assumes that the propagation velocities of the leading edge ($0.9V_\infty$) and the trailing edge ($0.5V_\infty$) differ and that the resulting turbulent band eventually merges with the adjacent ones to form a turbulent BL. In their experiments, Kittichaikarn et al. (1999) visualize that wake-induced transition actually starts with the formation of turbulent spots. An excellent overview of modeling unsteady transition on turbine blades is provided by Hodson (1998).

With respect to modeling BL transition with periodic wake passing and base turbulence, it is often argued that the amplitudes of the laminar BL caused by stochastic fluctuations in the base flow and/or in the periodic wake are so high that linear instabilities such as the Tollmien-Schlichting waves can no longer occur and that – for this reason – the linear stability theory cannot be used for modeling the transition behavior. Of course we cannot expect that within a specified time and a given space, amplitudes of unlimited size are fully dampened by the laminar BL. In this paper, it is argued that due to acceleration and decay of turbulence along the suction side of LPT blades, the turbulence level from the inflow is lowered to a level that allows laminar regions in the transitional flow to exist. Additionally, there are high pressure gradients following the acceleration in the transition region of LPTs. According to Herbert (1993), the region of linear instability dominates in length over non-linear regions and subsequent stages up to the fully developed turbulent BL. Thus, the beginning of transition might be correctly determined by calculating the end of the linear region. This may be done using the e^N method derived from the linear stability theory, with the selected exponent indicating the initial disturbance in the laminar BL, which in turn depends on the turbulence level of the outside flow. Provided that the beginning of transition has been determined fairly correctly, the associated change in profile loss can be calculated as a function of time. Ultimately, this is based on the idea that the periodic transition behavior of LPTs also represents a stability problem of the laminar BL.

So far it has not been possible to clarify definitely why the wake from the upstream blade row should disturb the BL in the area near the wall as it penetrates only the outermost regions. If the wake strikes the leading edge of the downstream row, it is first decelerated in the stagnation point flow and then accelerated by the laminar BLs forming on the pressure and suction sides. When the wake is accelerated along the suction side of a turbine airfoil, it is assumed that all disturbances of the wake in the near-wall BL have died out. A possible explanation of how

transition can be caused by increased disturbances in the near-wall BL might be derived from the "receptivity" theory. It is based on the assumption that a mode conversion takes place, i.e. that energy of disturbances from the outermost region of the BL is transferred to modes in the near-wall BL (Morkovin, 1985).

The remaining challenge is now to develop a numerical model accurate enough to account for wake interaction effects while keeping the balance between model resolution and computing costs (Adamczyk, 1999). As the direct numerical solution exceeds today's computer capabilities by far and simple mean-line models are insufficient for the blade design process, an improvement of semi-empirical models seems to be the first goal, eventually leading to a modeling free of empirical input for the future. The experimental database, especially at off-design operating conditions at low Reynolds numbers, is built within the framework of the investigation reported in this paper.

EXPERIMENTAL APPARATUS

Turbine Cascade

The reported measurements were performed on a large scale LPT cascade (Fig. 1) consisting of 5 aft-loaded blades which represent the mid-span section of the PW2037 LPT rotor. As the objective was to increase the lift coefficient by about 30 %, blade pitch was raised to t/l=1.05 as compared with design point conditions (t/l=0.799) to achieve a higher blade loading. The blade geometry was not adapted accordingly and a large separation bubble formed on the suction side starting at approximately 60% axial chord (see Fig. 4).

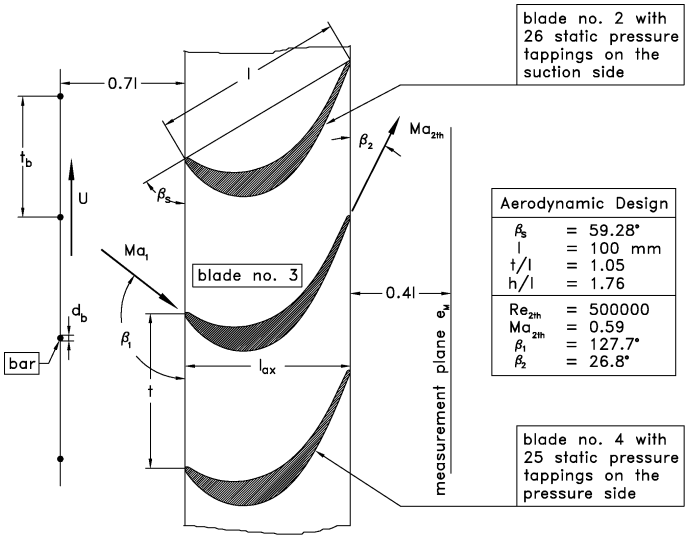

Fig. 1: T106D cascade design

Test Facilities

All experimental data presented in this paper were obtained using the High Speed Cascade Wind Tunnel of the Universität der Bundeswehr München. This continuously operating open loop facility is situated inside a large pressurized tank and can reach Mach numbers of up to Ma=1.05 in the test section. It allows Mach and Reynolds numbers to be varied independently in order to achieve flow conditions typical for modern gas turbines. The turbulence intensity in the test section can be adjusted using different turbulence grids upstream of the nozzle. A detailed description of the facility can be found e.g. in Sturm et. al. (1985).

The influence of the upstream blade row on the turbine cascade was simulated by using a moving bar wake generator with a bar diameter ratio of $d_b/l=0.02$. The cylindrical steel bars create a far wake very similar to the one produced by an actual airfoil (Pfeil and Eifler, 1976). The distance ratio between the bars and the cascade inlet plane is about x/l=0.7 (see Fig. 1). The belt mechanism drives the bars with speeds of up to 40 m/s, thus generating Strouhal numbers between 0.42-1.68 for the investigated test cases. This so-called EIZ and its constructional principles are explained by Acton and Fottner (1997) in greater detail.

Measurement Techniques

The aerodynamic performance at different operating points was evaluated by measuring stagnation pressure losses with a pitch-wise traversing five-hole probe (for steady-state conditions) or a wake rake (for unsteady conditions) in a plane $e_M/l=0.4$ (see Fig. 1) downstream of the cascade exit plane. A conventional pitot probe was used to determine the inlet stagnation pressure. Static pressure tappings on both the suction and the pressure side at midspan were connected to a Scanivalve system and allowed the surface pressure distribution and therefore the blade loading to be measured. All pneumatic data were recorded via computer control and represent mean values, therefore making a time-resolved study of loss behavior impossible.

Arrays of surface-mounted hot film sensors were glued onto the suction side of blade no. 3 to analyze the development of the BL characteristics along the profile over time. The entire length of the suction surface was covered with a total of 36 gauges with their spacing varying between 2.5 and 5 mm. They consisted of a 0.4 µm thin nickel film applied by vapour deposition process onto a polyamide substrate and were logged simultaneously in sets of 12 sensors at sampling frequencies ranging from 40 to 60 kHz. The frequency response of the sensors was sufficient to resolve the first two harmonics of the bar passing frequency. As shown e.g. by Schröder (1991), the BL characteristics can be determined directly from the anemometer output and do not necessarily require an extensive calibration procedure. The CTA anemometer data was low-pass filtered and digitized with a 12-bit A/D-converter before being stored on hard disks. A once-per-revolution trigger mechanism ensured that the wake passing effects were studied for wakes produced by identical bars.

In the cascade inlet plane, a standard 1D hot wire probe was used to measure the turbulence intensity inside and outside the wake and the velocity deficit caused by the bars. Calibration was performed in-situ for each operating point before running the experiment using a 4^{th} order polynomial. The number of points was large enough to correctly reproduce the slope of the calibration curve for the calculation of the turbulence level. Oil-and-Dye pictures were taken at selected operating conditions to ensure that the flow field at midspan was two-dimensional and unaffected by secondary flow effects.

Data processing for the hot film and hot wire data was done using the well-established PLEAT technique (Phase Locked Ensemble Averaging Technique, Lakshminarayana et al., 1974) in order to separate random and periodic signals. A total of 300 ensembles was logged with each run and evaluated for quasi-wall shear stress (Eq. 1), random unsteadiness RMS (Eq. 2) and skew (Eq. 3), where b represents the anemometer output voltage for the hot film results. To be able to compare

the hot film sensors, the resulting values were normalized with the anemometer voltage at zero flow, thereby eliminating the influence of manufacturing differences between the gauges.

$$\tilde{b}(t) = \frac{1}{n} \cdot \sum_{j=1}^{n} b_j(t) \hat{\approx} \frac{E(t) - E_0}{E_0} \quad (1)$$

$$\sqrt{\tilde{b}^2(t)} = \sqrt{\frac{1}{n-1} \cdot \sum_{j=1}^{n} (b_j(t) - \tilde{b}(t))^2} \hat{\approx} \frac{E_{RMS}(t)}{E_0} \quad (2)$$

$$\mu_3(t) = \frac{1}{(\tilde{b}(t))^3} \cdot \frac{1}{n-1} \cdot \sum_{j=1}^{n} (b_j(t) - \tilde{b}(t))^3 \quad (3)$$

For the hot wire data, the ensemble-averaged turbulence level was calculated from the calibrated velocities c according to Eq. 4.

$$\tilde{Tu}(t) = \frac{1}{\tilde{c}(t)} \cdot \sqrt{\frac{1}{n-1} \cdot \sum_{j=1}^{n} (c_j(t) - \tilde{c}(t))^2} \quad (4)$$

A typical result of the hot wire measurements is shown in Fig. 2 and served as input data for the numerical calculations. Values for the velocity deficit, the turbulence level and the wake width can easily be extracted from the figure. For cases with increased bar pitch, non-disturbed flow sections between the wakes were used to determine the background turbulence level with (approx. 2.2%) and without grid (≤ 1%).

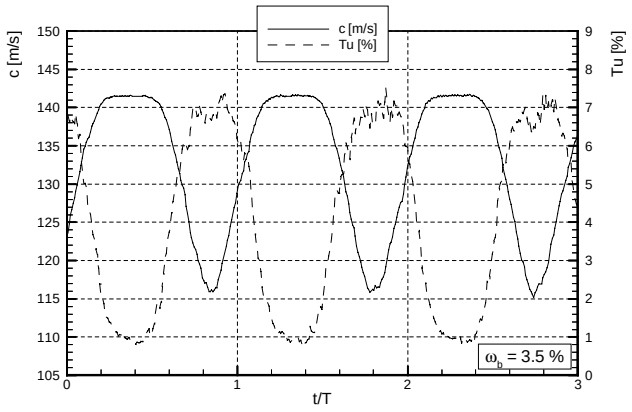

Fig. 2: Data of the 1D hot wire measurements at Re_{2th} = 200.000, Ma_{2th} = 0.4, U_b = 20 m/s, t_b = 40 mm, Sr = 0.84, with grid

MATHEMATICAL MODELING

To better understand the physical process which plays an important part in transition and to separate specific regions from each other, the characteristic directions are determined in space-time diagrams of wall shear stress derived from experimental data. As these characteristic directions should also be present in numerically correct simulations, the "Unsteady Boundary Layer Interaction Method" (UBLIM) was extended by replacing the previously used solution algorithm by Arndt (1991) with the "Split coefficient matrix method" by Chakravarthy (1979). This method utilizes information of signal propagation provided by the method of characteristics. The momentum equation and the mechanical energy equation are rearranged so that a first-order system of coupled quasi-linear partial differential equations (Eq. 5) is obtained.

$$\frac{\partial \vec{u}}{\partial t} + [A] \frac{\partial \vec{u}}{\partial x} = \vec{r} \quad (5)$$

The column vector $\vec{u} = (\theta, H)^T$ is the dependent variable of the two unknowns momentum thickness θ and shape factor H. The independent variables are t and x. [***A***] is a 2x2 coefficient matrix, whose elements as well as the lengthy components of vector $\vec{r} = (r_1, r_2)^T$ are given in appendix A. The components of the right hand side contain temporal and space derivatives which are given quantities for each time-step at the edge of the BL. The boundary condition for $\vec{u}$ at (t, 0) is given by the stagnation point flow and the condition for $\vec{u}$ at (t, x_{max}) is given with no upstream influence present. The initial condition for $\vec{u}$ (0, x) is given by the BL of the infinite plate. The system of equations is hyperbolic as the eigenvalues of [***A***] over the whole solution domain are real and distinct. The eigenvalues or the directions of information in the BL as roots from the characteristic equation are given by Eq. 6 as

$$\lambda_{1,2} = \left(\frac{dx}{dt} \right)_{1,2} = u_e \left(-\frac{p}{2} \pm \sqrt{\frac{p^2}{4} - q} \right) \quad (6)$$

where u_e represents the velocity at the edge of the BL, p and q are functions of $\vec{u}$, see appendix A.

If the flow is attached, the signs of the first and second eigenvalue are positive. For a separated flow, the sign of the first eigenvalue is positive again, but the sign of the second eigenvalue is negative, which means that the signal propagation is on the one hand downstream and on the other hand upstream and influences the solution in that way. The eigenvalues correspond to characteristic velocities, whose paths result in characteristic directions in the space-time diagrams, see Fig. 3.

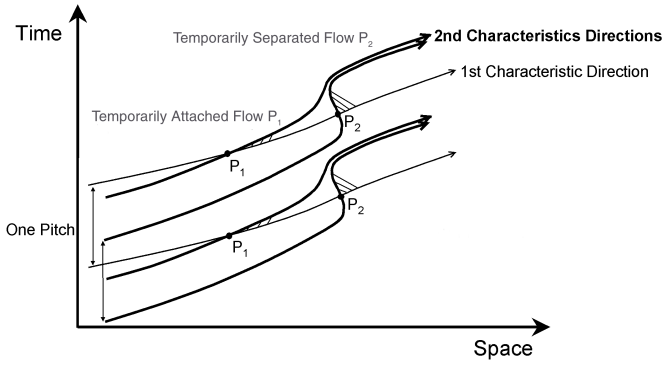

Fig. 3: Regions of influence for attached and temporarily separated flow

Although mathematically the unsteady BL has the two independent variables t and x, the problem is often called one-dimensional, meaning one dimension in space, with the second space dimension y

normal to the wall being eliminated by integrating in this direction. Considering the two dependent variables θ and H, there are only two characteristic directions of the BL that can be followed by disturbances. These disturbances have to occur at frequencies higher than the frequency of the BL itself to follow these characteristic directions. Thus the frequency is expected to be smaller than the characteristic frequencies of turbulence so that the modulation of turbulence by the driving unsteady phenomenon should be negligible. While in an attached flow, disturbances affect only a relatively small zone, their region of influence is spread out in temporaily separated flow.

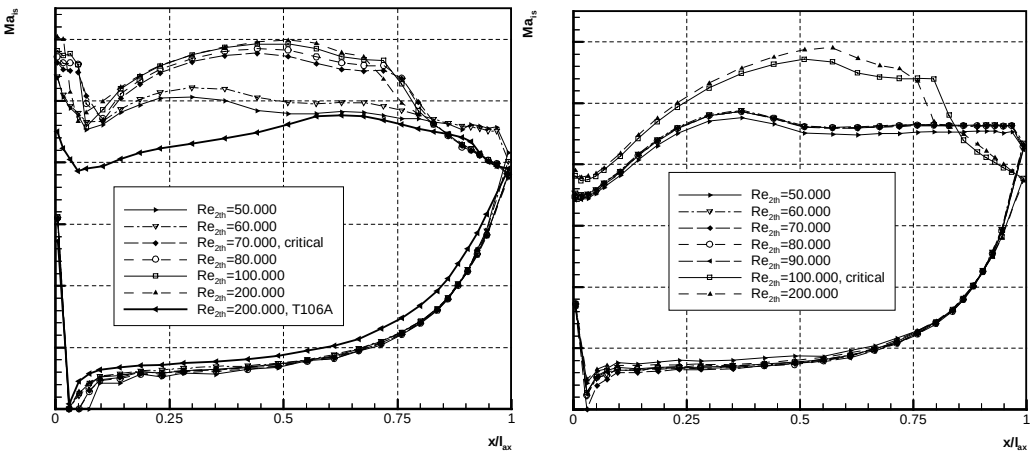

Fig. 4: Isentropic Mach number distribution for steady inflow, β_1 = 132.7° (left) and β_1 = 122.7° (right)

For better understanding, the essential statements are illustrated in Fig. 3. While in the attached flow region (P_1) disturbances influence only a relatively small region downstream following two characteristic directions of propagation, such disturbances affect both downstream and upstream regions at the time the separation bubble occurs (P_2). This means that all disturbances in the second direction of propagation generated during one blade passing period arise nearly simultaneously at one single time step downstream whereas at all other times downstream disturbances are not possible.

TEST PROGRAM

The purpose of this investigation was to enhance the understanding of BL transition under the influence of wakes at design and off-design conditions. In a first step, a cascade called T106A with blades spaced at design pitch was examined at different Reynolds and Mach numbers with and without the wake generator. A small separation bubble formed in the rear part of the suction side, but was difficult to inspect with the hot film sensors due to its size. Results of these measurements are not shown in this paper.

Ma_{2th} \ Re_{2th}			**60.000** no grid	**60.000** w\ grid	**200.000** no grid	**200.000** w\ grid
0.4	U_b=0 m/s (steady)		■◆●	◆●	■◆●	●
	U_b=20 m/s	t_b=40 mm	■◆●	-	■◆●	-
		t_b=80 mm	■◆●	◆●	■◆●	-
	U_b=40 m/s	t_b=40 mm	■◆●	-	■◆●	-
		t_b=80 mm	■◆●	◆●	■◆●	-
0.59	U_b=0 m/s (steady)		■◆●	◆●	■◆●	●
	U_b=20 m/s	t_b=40 mm	■◆●	-	■◆●	-
		t_b=80 mm	■◆●	◆●	■◆●	-
	U_b=40 m/s	t_b=40 mm	■◆●	-	■◆●	-
		t_b=80 mm	■◆●	◆●	■◆●	-

■ casc. T106A ◆ casc. T106D, β_1=122.7° ● casc. T106D, β_1=132.7°

Tab. 1: Cascade test program

As previous investigations suggest that a higher blade loading is possible when considering the beneficial influences of wake interaction, the cascade T106D with increased blade pitch as described above was built without modifying the profile geometry. To get an idea of the increase in blade loading, the isentropic Mach number distribution of the old cascade T106A is shown in Fig. 4 (left). Tests included measurements at different Reynolds and Mach numbers, background turbulence intensity levels (with and without grid) and inlet flow angles. Unsteady flow characteristics were varied by changing the bar pitch and the bar velocity of the wake generator. A complete set of all studied parameters is compiled in Tab. 1. However, the present paper will focus on results obtained at Ma_{2th}=0.4.

EXPERIMENTAL RESULTS

Measurements under steady conditions

Before using the wake generator, measurements were performed under steady-state conditions, i.e. without bars at a background turbulence level of about 1%. Fig. 4 shows the isentropic Mach number distribution at Ma_{2th}=0.4 for varying Reynolds numbers at the flow angle β_1=132.7° (left). Massive separation – i.e. bursting of the separation bubble – occurs on the suction side for Reynolds numbers less than 70.000 whereas the pressure side seems to be almost unaffected except for the location of the stagnation point. At a characteristic Reynolds number, the BL is able to reach the back pressure at the trailing edge and a large separation bubble forms. As expected, the size of the bubble decreases with increasing Reynolds number. It should be noted that for these measurements, the wake generator was already installed, but with no bars present in front of the cascade inlet plane. Small gaps at the upper and lower end of the cascade were necessary to move the bars, which resulted in a loss of mass flow. The resulting change in flow angle was calculated numerically to be about +5°. Therefore there is a discrepancy between the inlet flow angle β_1 and the geometrical angle of the setup which was the design angle of the old cascade (β_1 = 127.7°). The combination of mass flow leakage and increase in profile lift coefficient results in a large suction peak which is clearly visible in Fig. 4, left. No measurements were performed for the old design angle of the profile T106 (see Fig. 1).

At an inlet angle of β_1=122.7°, the massive separation is even more obvious, but now up to a characteristic Reynolds number of

90.000 (Fig. 4, right). Compared to β_1=132.7°, the maximum isentropic Mach number values reached on the profile remain almost constant and the position of the bubble moves downstream.

Data for unsteady inflow

Ensemble-averaged RMS results of the hot-film measurements at Ma_{2th}=0.4, Re_{2th}=200.000 are shown in Fig. 5 using space-time diagrams. Non-dimensionalized wake passing time along the ordinate is plotted over non-dimensionalized axial chord length along the abscissa, which allows the propagation velocity of phenomena caused by the wakes to be extracted directly from the experimental data. Red areas indicate maximum and blue regions minimum values. As the data is mapped only qualitatively, the measured RMS and shear stress values do not correspond to reality.

In the RMS plots, the continuous black line represents zero skewness which is used to identify the transition point (Halstead et al, 1997b). The location of the transition point under steady state conditions determined from hot film measurements is shown as a continuous white line and denoted as TP_{stat}. The first operating point for unsteady inflow serves as a reference for all future comparisons and is therefore discussed in more detail.

The incoming wake hits the leading edge of the blade at point (**1**) and is easily identifiable by large RMS values resulting from the high turbulence intensity. The wake width matches the results of the 1D hot wire measurements (see Fig. 2). Between the wakes, a small separation bubble (**2**) characterized by higher RMS values (and visible in oil-and-dye pictures) forms, but subsequently relaminarizes due to the acceleration on the suction side. This is also evident in Fig. 6 (left) where the values of skew are plotted. Up to about x/l_{ax} = 0.4, the character of the BL remains laminar. At this position, the wake path becomes visible again and triggers the transition process which is in phase with the wake. Disturbances in the wake penetrate the laminar BL and initiate turbulent spots (Mayle and Dullenkopf, 1990). According to measurements by Schubauer and Klebanoff (1955) at zero pressure gradient, the leading edge of the turbulent spots moves at about 0.88 times the free stream velocity whereas the trailing edge only reaches values around $0.5V_\infty$.

Following the transitional strip, the so-called becalmed region (**B**) – characterized by decreasing RMS values – is less susceptible to external disturbances and delays the onset of transition (Halstead et al., 1997a). Its trailing edge travels at a speed of approximately $0.3V_\infty$. The corresponding trajectories are plotted in the figure and reasonably match those given in the literature by other researchers. It can be observed that the transition point (black line) moves upstream as compared with steady state conditions (continuous white line) in the wake-induced path (**A**) and downstream in the region affected by calming (**D**).

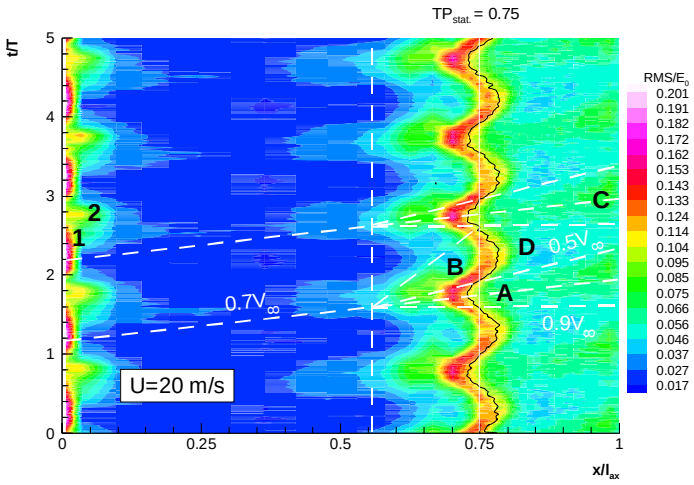

Fig. 5: Hot film RMS values at Re_{2th} = 200.000, Ma_{2th} = 0.4, t_b = 40 mm, U_b = 20 m/s, β_1 = 132.7°, Sr = 0.84

Obvious discrepancies between the location of a "time-integrated" transition point for unsteady conditions and the position of the transition point for steady conditions can be explained by the isentropic Mach number distribution in Fig. 6. The use of the wake generator changes the inlet velocity triangle a little and results in a different Mach number distribution on the suction side. When the transition process is complete, the wake-induced transitional strip becomes a turbulent one (**C**). However, it should be noted that all boundaries are idealized as straight lines which is not exactly true as the freestream velocity varies with the airfoil passage. Skewness displays a behavior typical for transition with laminar separation bubble (for details see Halstead et al., 1997b).

Supplementary information can be extracted from the ensemble-averaged contour plots of quasi-wall shear stress (Fig. 11, upper left plot). The position of the separation bubble identifiable by low shear stress (blue regions) coincides with the one in the

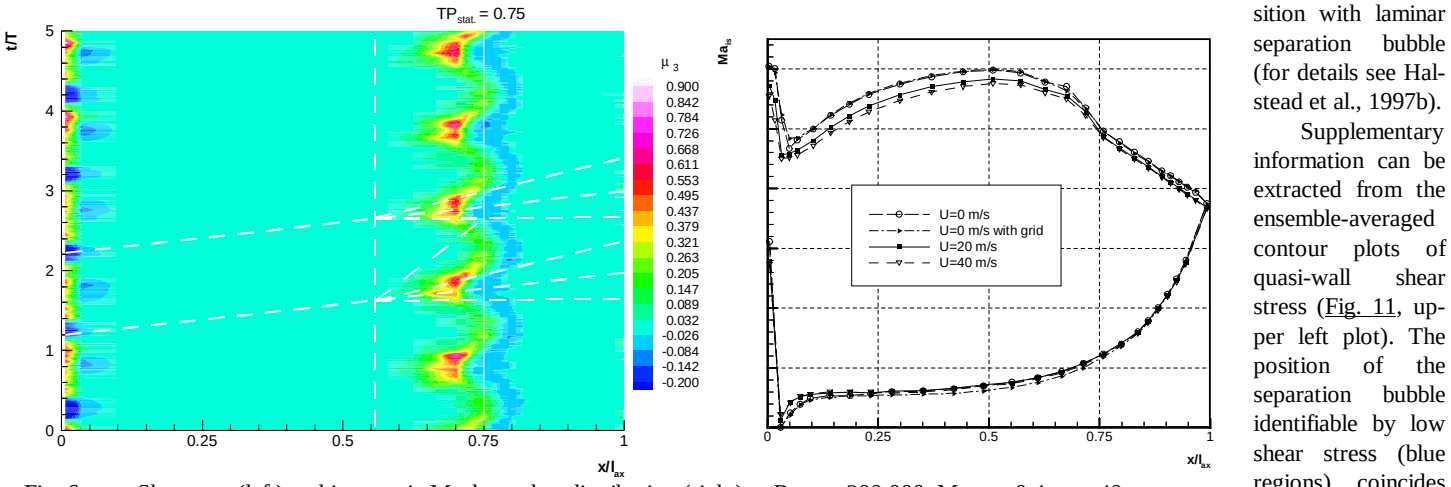

Fig. 6: Skewness (left) and isentropic Mach number distribution (right) at Re_{2th} = 200.000, Ma_{2th} = 0.4, t_b = 40 mm, U_b = 20 m/s, β_1 = 132.7°, Sr = 0.84

Mach number distribution (Fig. 6, right) and decreases in size with increasing wake passing frequency (not shown). The isentropic Mach number distribution includes additional results with the turbulence grid installed and shows the influence of an increased wake passing frequency. Higher levels of background turbulence reduce the size of the separation bubble whereas the change in bar speed affects the inlet velocity triangle. The latter leads to a smaller suction peak and consequently to lower maximum velocities on the suction side. The pressure side seems to be almost unaffected.

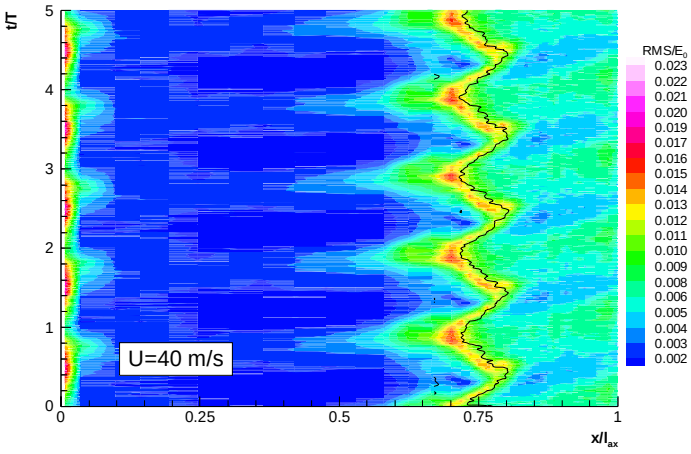

Fig. 7: Hot film RMS values at Re_{2th} = 200.000, Ma_{2th} = 0.4, t_b = 80 mm, U_b = 40 m/s, β_1 = 132.7°, Sr = 0.84

A comparison of Fig. 7 with Fig. 5 illustrates the influence of varying bar pitch and bar speed simultaneously. Pitch and speed were doubled to t_b=80 mm and U_b=40 m/s, respectively, while the Strouhal number of Sr=0.84 remained constant. While the mean location of the transition point is hardly changed, the shape of the transition onset and the extent of the becalmed region is completely different.

Hot film data for Re_{2th}=60.000, which corresponds to conditions typically encountered in LP turbines at high altitude cruise level, is displayed in Fig. 8. Bar pitch remained at t_b=80 mm to reduce the wake passing frequency and, thus, to make the plot more clear. As observed by Halstead et al. (1997b), the wake-induced transitional strips move towards the trailing edge with decreasing Reynolds number. The same is true for the whole transitional region characterized by high RMS values. Contrary to Halstead's findings, the wake-induced transitional strips are clearly visible in the laminar region and by no means weak. A local RMS maximum (**E**) characteristic for the separation point is now visible upstream of the global maximum. The effects of the becalmed region (**F**) following the wakes are extremely pronounced. Values of zero skewness could not be detected over the whole surface length.

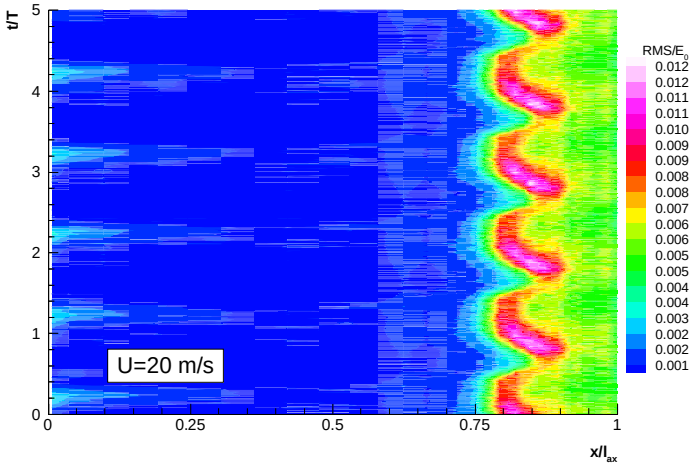

Fig. 9: Hot film RMS values at Re_{2th} = 60.000, Ma_{2th} = 0.4, t_b = 80 mm, U_b = 20 m/s, β_1 = 122.7°, Sr = 0.42

Due to the increased turbulence level induced by the wakes, the BL seems to attach as demonstrated with the isentropic Mach number distribution (Fig. 8, right), but the available data represents only *mean* values and has to be treated with care. Nevertheless it is obvious that with increasing wake passing frequency (Strouhal number) the extent of the separation bubble decreases. An elevated level of turbulence prevents the massive separation observed for steady state conditions even when no wakes are present.

The influence of a change in the inlet flow angle to β_1=122.7° is shown in Fig. 9. As seen from the isentropic Mach number distribution for steady state conditions (Fig. 4), there is no suction peak and no leading edge separation bubble. The continuous acceleration leads to a very stable laminar BL up to x/l_{ax}=0.75, where transition is in-

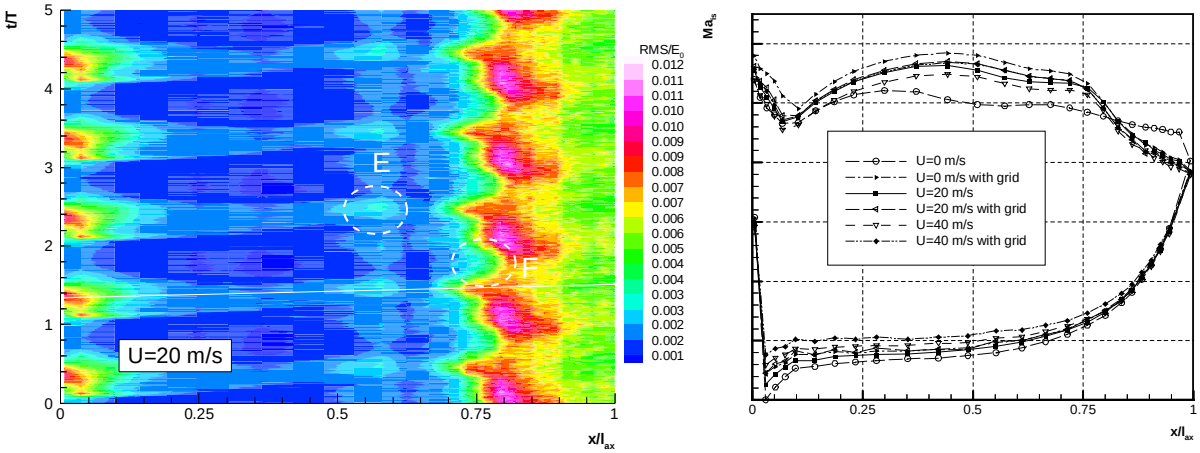

Fig. 8: Hot film RMS values (left) and corresponding isentropic Mach number distribution (right) at Re_{2th} = 60.000, Ma_{2th} = 0.4, t_b = 80 mm, U_b = 20 m/s, β_1 = 132.7°, Sr = 0.42

duced by the wake path, which is clearly visible by the periodic onset of transition. Compared to Fig. 8, the maximum RMS values occur closer to the trailing edge which indicates that the transitional region moves downstream.

Stagnation pressure losses

The aerodynamic performance of the blade was judged by computing the profile loss coefficient ω (Eq. 7)

$$\omega = \frac{p_{t1} - \overline{p_{t2}}}{p_{t1} - p_2} \qquad (7)$$

where p_{t2} is the averaged exit stagnation pressure. As the pitot probe used for measuring p_{t1} was located upstream of the bars, the recorded values of p_{t1} were corrected by the bars' stagnation pressure loss.

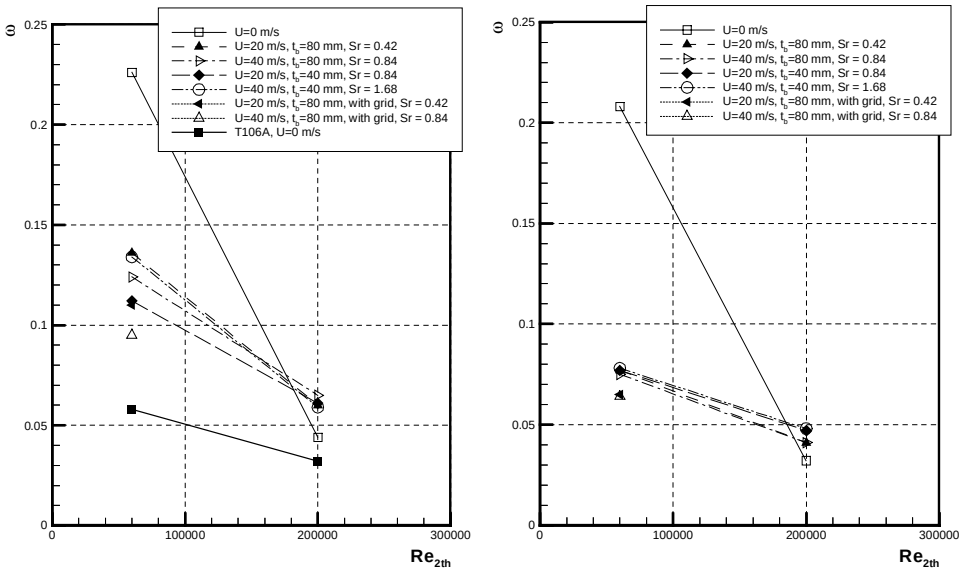

Fig. 10: Loss coefficients for a variation of Strouhal and Reynolds number at Ma_{2th} = 0.4, β_1 = 132.7° (left) and β_1 = 122.7° (right)

In Fig. 10, the calculated values for ω are plotted versus the Reynolds number for the two inlet flow angles. The increased blade loading for the cascade T106D leads to overall stagnation pressure losses that are higher than the values recorded for the cascade T106A. At Reynolds numbers of Re_{2th} = 200.000, the increased level of turbulence by the wakes results in higher losses as compared with steady-state conditions. This is independent of the inlet flow angle and implies that the beneficial effect of calming is outbalanced by the earlier onset of transition. For Re_{2th} = 60.000, losses are reduced if the blades are subjected to wakes. However, minimum losses are obtained for the combined use of wake generator and turbulence grid, which indicates that there is potential for further optimizations. Loss reduction is larger at higher Mach numbers (not shown in the paper).

NUMERICAL RESULTS

An important technical achievement is the reduction of complex relationships to simple models that – despite their simplicity – truly reflect the essential physical effects of the significant flow quantities. In order to compute the losses in a blade row of a multi-stage LPT, it is necessary to simulate the transition process from laminar to turbulent flow of the BL under periodic conditions on the suction side. Turbulent flow in this sense means that the process of transition is completed to form a periodic turbulent BL. So the first simplification made for the calculations is not to resolve the small scale turbulence and the time-variant large-scale structures (LES) but to remain at the level of a turbulence model. Secondly, the calculation should be limited to a BL and, thirdly, to an integral calculation method.

A method for calculating quasi three-dimensional BLs in multi-stage LPTs is briefly described in the following. The amplitudes for velocity, pressure and density are determined using the linearized Euler method (Kahl, 1993) having used the quasi three-dimensional stationary Euler solution. The amplitudes of the turbulence level at the edge of the BL are calculated on the basis of the experimentally determined laws of decay for turbulence and wake using the values of the turbulence level at the cascade inlet plane (Fig. 2). Phases are derived from the vorticity calculated by the linearized Euler solution. After these steps, velocity, pressure, density and turbulence level are known for any point in time and are used as input values for the BL calculation. The turbulence level serves as input value for N for the e^N method used. As calibrations with MTU's test rigs show, the applicability of this method has its limits in cases where – owing to viscosity effects and changed displacement body – the outflow direction differs markedly from the direction determined for an inviscid flow.

For the "reference" point, numerical calculations using this method have been performed for two different bar speeds and two different bar pitches with the Strouhal number remaining constant. The numerical results of quasi wall shear stress are in good agreement with the experimental data as can be seen in Fig. 11. In addition, the calculations include plotted light lines of the second characteristic direction of propagation of disturbances. They start at different times spaced by one fifth of a blade passing period from a position near the blade leading edge. It is obvious that these disturbances do not affect the temporarily separated region but penetrate the region where the transition has reached its farthest upstream position. The meridional system M/M_{ges} employed for the spatial direction is identical to the previously used axial system x/l_{ax}. As the sensitivity of the hot film sensors differs between the laminar and the turbulent part of the BL, the calculated numerical values of wall shear stress should be corrected in the transitional and turbulent regions for future work.. This was not done for Fig. 11.

CONCLUSIONS

A highly loaded LPT cascade blade was subjected to wakes shed by upstream bars in order to simulate turbomachinery conditions. The effects of varying Reynolds and Strouhal number as well as inlet flow angle on wake-induced transition were studied. Preliminary steady-state flow tests showed massive separation at low Reynolds numbers, resulting in a dramatic increase in profile loss. Separation could be at

least partially prevented by unsteady inflow conditions, thereby reducing the profile pressure loss coefficient.

- Identical Strouhal numbers obtained by anti-cyclically varying bar pitch and bar speed produced different effects on the BL. Therefore, the wake passing frequency cannot be the only determinant parameter for the simulation of rotor-stator interaction. It is evident that the ratio of upstream bar pitch and cascade pitch plays the other key role.
- Starting at a characteristic Reynolds number, massive separation occurs under steady state conditions. This Reynolds number depends on the inlet flow angle and decreases with increasing angle of attack.
- The BL development depends on the frequency and the strength of the wake. Wake passing is more effective at low Reynolds numbers, high Mach numbers and at off-design conditions as it helps to prevent laminar separation.
- While in an attached flow disturbances in the BL affect a relatively small region of influence downstream in two characteristic directions, such disturbances become effective both in downstream and upstream direction at the time the separation bubble forms. All disturbances following the second direction of propagation which have been generated during one blade passing period occur nearly simultaneously at one single point in time downstream, whereas at all other times downstream disturbances are not possible.

It is highly probable that with decreasing Reynolds number the angle between the detaching streamline and the wall increases to a certain degree or, in other words, the quotient of the wall shear stress and the pressure gradient at laminar can only increase up to a certain value, see Fiala (1999). For a pressure gradient at laminar separation gradually approaching zero with decreasing Reynolds number (see Fig. 8), the BL velocity profile becomes less destabilized and, as a consequence, parts of the amplitudes of disturbances are dampened and their effects on transition are more and more diminished.

Further work is needed to clarify these suppositions. Finally the questions have to be settled why the transition process is not completed with decreasing Reynolds number near massive separation and how the

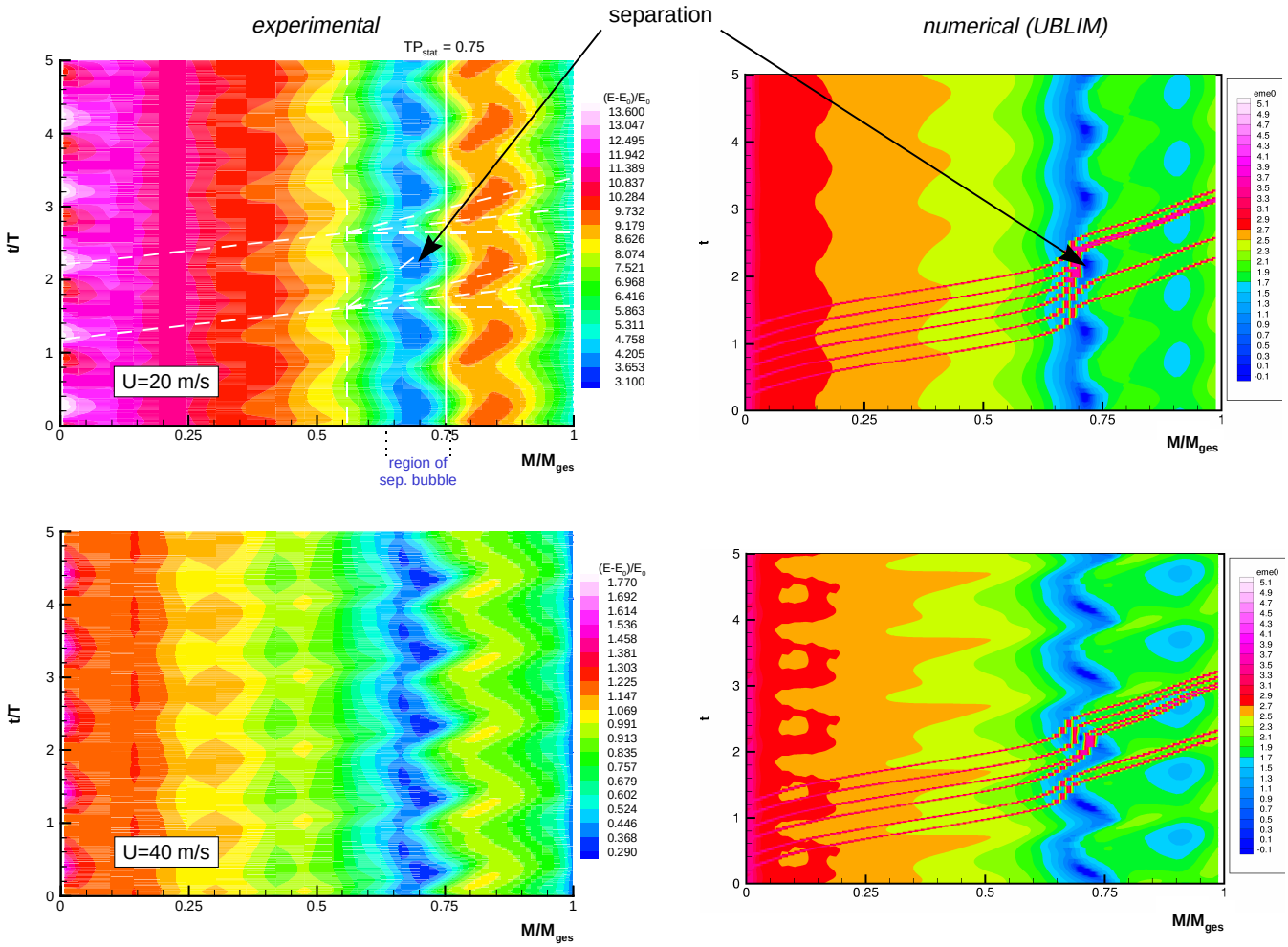

Fig. 11: Comparison of quasi wall shear stress from experimental and numerical results at Re_{2th} = 200.000, Ma_{2th} = 0.4, β_1 = 132.7°, Sr = 0.84

effects of wake passing can influence the start of massive separation encountered for very low Reynolds numbers.

ACKNOWLEDGMENTS

The work reported in this paper was funded within the framework of the "Engine3E Programm". The support and the permission for publication are gratefully acknowledged.

REFERENCES

Acton, P., Fottner, L., (1997), "Investigation of the Boundary Layer Development on a Highly Loaded Low Pressure Turbine Cascade under the Influence of Unsteady Flow Conditions", Proceedings of the 8th International Symposium on Unsteady Aerodynamics and Aeroelasticity of Turbomachines, Stockholm

Adamczyk, J.J., (1999), "Aerodynamic Analysis of Multistage Turbomachinery Flows in Support of Aerodynamic Design", ASME Paper 99-GT-80

Arndt, N., (1991), "Beschreibung eines Rechenprogramms für Grenzschichtrechnungen (Turbotech-Aufgabe 1.1.3.1)", Technische Notiz, MTUM-N91EW-0022

Chakravarthy, S.R., (1979), "The Split-Coefficient Matrix Method for Hyperbolic Systems of Gasdynamic Equations", Ph.D. dissertation, Department of Aerospace Engineering, Iowa State University, Ames

Fiala, A., (1999), "Auslegungskriterium 'Reynoldszahl bei Aufplatzen der Ablöseblase'", Technische Notiz, MTUM-N99TPKE-004

Halstead, D.E., Wisler, D.C., Okiishi, T.H. Walker, G.J., Hodson, H.P., Shin, H.-W., (1997a), "Boundary Layer Development in Axial Compressors and Turbines, Part 1 of 4: Composite Picture", ASME Journal of Turbomachinery, Vol. 119, pp. 114-127

Halstead, D.E., Wisler, D.C., Okiishi, T.H. Walker, G.J., Hodson, H.P., Shin, H.-W., (1997b), "Boundary Layer Development in Axial Compressors and Turbines, Part 3 of 4: LP Turbines", ASME Journal of Turbomachinery, Vol. 119, pp. 225-237

Herbert, T., (1993),"Parabolized Stability Equations", AGARD-R-793, 4-1, pp 4-29, Special Course on Progress in Transition Modeling

Hodson, H.P., (1984), "Boundary Layer and Loss Measurements on the Rotor of an Axial Flow Turbine", ASME Journal of Engineering for Gas Turbines and Power, Vol. 106

Hodson, H.P., (1989), "Modeling Unsteady Transition and its Effects on Profile Loss", AGARD CP 468

Hodson, H.P., Addison, J.S., Shepherdson, C.A., (1992), "Model for Unsteady Wake-Induced Transition in Axial Turbomachines", Journal de Physique III, Vol. 2, pp. 545-574

Hodson, H.P., (1998), "Blade Row Interference Effects in Axial Turbomachinery Stages", Von Karman Institute for Fluid Dynamics Lecture Series 1998-02

Kahl, G., Klose, A.,(1993),"Computation of Time-linearized Transonic Flow in Oscillating Cascades", ASME Paper 93-GT-269

Kittichaikarn, C., Zhong, S., Hodson, H.P., (1999), "An Investigation on the Onset of Wake-Induced Transition and Turbulent Spot Production Rate Using Thermochromic Liquid Crystals", ASME Paper 99-GT-126

Lakshminarayana, B., Poncet, A., (1974), "A Method of Measuring Three-Dimensional Rotating Wakes behind Turbomachinery Rotors", ASME Journal of Fluid Engineering, Vol. 96, pp. 87-91

Mayle, R.E., Dullenkopf, K., (1990), "A Theory for Wake-Induced Transition", ASME Journal of Turbomachinery, Vol. 112, pp. 188-195

Morkovin, M.V., (1985), "Bypass Transition to Turbulence and Research Desiderata", Transition in Turbines, NASA Conference Publication 2386, p. 161-204

Pfeil, H., Eifler, J., (1976), "Turbulenzverhältnisse hinter rotierenden Zylindergittern", Forschung im Ingenieurwesen, Vol. 42, pp. 27-32

Pfeil, H., Herbst, R., Schröder, T., (1983), "Investigation of the Laminar-Turbulent Transition of Boundary Layers Disturbed by Wakes", ASME Journal of Engineering for Power, Vol. 105, pp. 130-137

Schröder, T., (1991), "Investigation of the Blade Row Interaction and Boundary Layer Transition Phenomena in a Multistage Aero Engine Low Pressure Turbine by Measurements with Hot-Film Probes and Surface-Mounted Hot-Film Gauges", Boundary Layers in Turbomachines, VKI Lecture Series 1991-6

Schubauer, G.B., Klebanoff, P.S., (1955), "Contributions to the Mechanics of Boundary Layer Transition", NACA TN 3489

Schulte, V., Hodson, H.P., (1998), "Unsteady Wake-Induced Boundary Layer Transition in High Lift Turbines", Journal of Turbomachinery, Vol. 120, pp. 28-35

Stadtmüller, P., (1999), "Untersuchung des Strömungsverhaltens von Turbinengittern mit Berücksichtigung von instationärer Zuströmung", Institutsbericht LRT-WE12-99/04, Institut für Strahlantriebe, UniBw München

Sturm, W., Fottner, L., (1985), "The High-Speed Cascade Wind Tunnel of the German Armed Forces University Munich", 8th Symp. on Meas. Techn. for Transonic and Supersonic Flows in Cascades and Turbomachines, Genoa

APPENDIX

1. Coefficients of matrix [*A*] and components of vector $\vec{r}$

For reasons of simplicity only the incompressible coefficients are given. Moreover, there was no adjustment of the dissipation coefficient c_d through an additional third partial differential equation for the maximal shear stress in the BL.

$$a_{11} = u_e\left(H_k^* - 1\right) \qquad a_{12} = u_e\theta\frac{dH_k^*}{dH_k}$$

$$a_{21} = \frac{u_e}{\theta}\left\{1 - H_k\left(H_k^* - 1\right)\right\} \qquad a_{22} = -u_e H_k\frac{dHk}{dH_k}$$

$$r_1 = -\frac{\theta}{u_e}\left(2 - H_k\right)\frac{\partial u_e}{\partial t} + \theta\left(H_k + 2 - 3H_k^*\right)\frac{\partial u_e}{\partial x} + 2u_e c_d - u_e\frac{c_f}{2}$$

$$r_2 = -\frac{H_k}{\theta u_e}r_1 - \frac{H_k}{u_e}\frac{\partial u_e}{\partial t} - \left(H_k + 2\right)\frac{\partial u_e}{\partial x} + \frac{u_e}{\theta}\frac{c_f}{2}$$

2. Constants in Eigenvalue expression

$$p = 1 - H^* - H_k\frac{dH_k^*}{dH_k} \qquad q = -4\frac{dH_k^*}{dH_k}$$

laminar: $H_0 = 4$

$$H_k \geq H_0 : \frac{dH_k^*}{dH_k} = 0.04\left(1 - \frac{H_0^2}{H_k^2}\right)$$

$$H_k \leq H_0 : \frac{dH_k^*}{aH_k} = -0.076\left(\frac{H_0^2}{H_k^2} - 1\right)$$

turbulent: $H_0 = \left[H_k(\mathrm{Re}_\theta)\right]_{c_f=0}$

$$H_k \geq H_0 : \frac{dH_k^*}{dH_k} = 0.04\left(1 - \frac{H_0^2}{H_k^2}\right) + 0.056\frac{H_k - H_0}{H_k - H_0 + 4/\ln \mathrm{Re}_\theta}$$

$$H_k \leq H_0 : \frac{dH_k^*}{dH_k} = -\left(0.165 - \frac{1.6}{\sqrt{\mathrm{Re}_\theta}}\right)\frac{H_0 + 0.6H_k}{H_k^2}(H_0 - H_k)^{0.6}$$

The matrix [*A*] is singular ($M_e<3.7$) for the stagnation point $u_e = 0$ or for the separation point $dH_k^*/dH_k = 0$. Therefore, the velocity at the edge of the BL is corrected by the displacement effect of the BL at the last time-step.